JOURNAL OF VIROLOGY, Feb. 2007, p. 1848–1857 Vol. 81, No. 4
0022-538X/07/$08.00+0 doi:10.1128/JVI.01967-06

Participation of both Host and Virus Factors in Induction of Severe Acute Respiratory Syndrome (SARS) in F344 Rats Infected with SARS Coronavirus▽

Noriyo Nagata,[1]* Naoko Iwata,[1] Hideki Hasegawa,[1] Shuetsu Fukushi,[2] Masaru Yokoyama,[3] Ayako Harashima,[1] Yuko Sato,[1] Masayuki Saijo,[2] Shigeru Morikawa,[2] and Tetsutaro Sata[1]

Departments of Pathology[1] and Virology I,[2] and Center for Pathogen Genomics,[3] National Institute of Infectious Diseases, Tokyo, Japan

Received 9 September 2006/Accepted 20 November 2006

To understand the pathogenesis and develop an animal model of severe acute respiratory syndrome (SARS)-associated coronavirus (SARS-CoV), the Frankfurt 1 SARS-CoV isolate was passaged serially in young F344 rats. Young rats were susceptible to SARS-CoV but cleared the virus rapidly within 3 to 5 days of intranasal inoculation. After 10 serial passages, replication and virulence of SARS-CoV were increased in the respiratory tract of young rats without clinical signs. By contrast, adult rats infected with the passaged virus showed respiratory symptoms and severe pathological lesions in the lung. Levels of inflammatory cytokines in sera and lung tissues were significantly higher in adult F344 rats than in young rats. During in vivo passage of SARS-CoV, a single amino acid substitution was introduced within the binding domain of the viral spike protein recognizing angiotensin-converting enzyme 2 (ACE2), which is known as a SARS-CoV receptor. The rat-passaged virus more efficiently infected CHO cells expressing rat ACE2 than did the original isolate. These results strongly indicate that host and virus factors such as advanced age and virus adaptation are critical for the development of SARS in rats.

The epidemic of severe acute respiratory syndrome (SARS) spread rapidly worldwide during the winter of 2003 to 2004 (16; http://www.who.int/csr/sars/country/en/). SARS-associated coronavirus (SARS-CoV) has been identified as the etiological agent of SARS (4, 5, 12, 14, 28). SARS-CoV has caused progressive respiratory failure and death of approximately 800 individuals, approximately 10% of over 8,000 patients (http://www.who.int/csr/sars/country/en/). Common symptoms of SARS are fever, nonproductive cough, myalgia, and dyspnea. An age of 60 years or older, comorbid disease, male sex, high neutrophil counts, and several biochemical abnormalities are associated with poor outcomes (1, 3, 16, 27, 38). Advanced age in particular is recognized as an independent correlate of adverse outcomes and a predictor of mortality.

Experimental animals, particularly monkeys, have been infected with SARS-CoV to analyze various pathogenic aspects of SARS according to Koch's postulates and to develop animal models to evaluate potential vaccines and antiviral agents (2, 5, 6, 7, 14, 17, 24, 30, 31, 34). Cats, ferrets, mice, pigs, guinea pigs, hamsters, chickens, and rats have also been investigated for SARS-CoV susceptibility (22, 23, 32, 33, 39). All these animals are susceptible to SARS-CoV after intrarespiratory inoculation and exhibit virus excretion in pharyngeal or nasal swabs, histopathological pulmonary lesions, and seroconversion. In monkeys, aged mice, and Syrian hamsters, infection is not lethal but results in consolidative pneumonitis that resolves within 1 week (7, 24, 30, 32, 33, 34). Thus, existing animal models are useful to analyze the pathology associated with early phases of SARS-CoV infection and to provide insights into early events in SARS-CoV infection.

The SARS-CoV spike (S) protein mediates the infection of receptor-bearing cells. In the case of several avian and mammalian coronaviruses, the S protein is cleaved by furin or a related protease into S1 and S2 proteins. The S1 protein bears the receptor attachment site, and the S2 protein mediates fusion activity (15). Angiotensin-converting enzyme 2 (ACE2) is a functional receptor for SARS-CoV that binds SARS-CoV S protein with a high affinity (18, 19, 20). Several reports suggest that ACE2 is a physiologically relevant receptor during infection. Its protein expression pattern corresponds to the localization of virus infection in humans and animals (10, 35). Also, the efficiency of infection in humans and other species correlates with the ability of ACE2 in that species to support viral replication (18, 21). Structural analysis of the peptidase domain of human, palm civet, mouse, and rat ACE2 with the SARS-CoV receptor-binding domain of S1 has identified aspects of that interface that enable efficient cross-species infection and human-to-human transmission (18). Interestingly, rat ACE2 does not support infection by SARS-CoV.

The objectives of this study were to understand the pathogenesis of and develop an animal model for SARS. We found that the Frankfurt 1 isolate of SARS-CoV replicated in the respiratory tracts of F344 rats without associated clinical symptoms. We passaged the Frankfurt 1 isolate serially in young F344 rats and found that by the 10th passage, the virus was altered such that it replicated more efficiently in rats than did the original virus. Furthermore, adult rats showed more severe acute lung injury than did young rats after infection with the passaged virus. Higher levels of cytokines were seen in adult

* Corresponding author. Mailing address: Department of Pathology, National Institute of Infectious Diseases, Gakuen 4-7-1, Musashimurayama, Tokyo 208-0011, Japan. Phone: 81-42-561-0771. Fax: 81-42-561-6572. E-mail: nnagata@nih.go.jp.

▽ Published ahead of print on 6 December 2006.

rats than in young rats after infection. Analysis of the nucleotide sequence of passaged virus encoding relevant S1 domains identified a missense mutation in the receptor binding domain. We found that this mutation is responsible for more efficient viral replication in rats. Comparative analysis of immune responses including an elevation in cytokine levels and histopathological findings in young and adult animals is crucial for understanding SARS pathogenesis.

MATERIALS AND METHODS

Viruses and cells. The SARS-CoV Frankfurt 1 isolate used here was kindly supplied by John Ziebuhr, Institute of Virology and Immunology, University of Würzburg, Würzburg, Germany. Virus was propagated twice in Vero E6 cells purchased from the American Type Culture Collection (Manassas, VA). Vero E6 cells were cultured in Eagle's minimal essential medium (MEM) containing 5% fetal bovine serum, 50 IU of penicillin G, and 50 μg of streptomycin per ml. Titers of this stock were expressed as 50% of the tissue culture infectious dose ($TCID_{50}$), which was calculated according to the Behrens-Kärber method using Vero E6 cells. Work with infectious SARS-CoV was performed under biosafety level 3 conditions.

Experimental infection of rats with SARS-CoV. F344 rats (4-week-old females purchased from Japan SLC, Inc.) were inoculated intranasally with SARS-CoV in a volume of 100 μl into the left nostril under anesthesia using an intraperitoneal injection of 0.1 ml/10 g body weight of 1.00 mg of ketamine (Ketalar) plus 0.02 mg of xylazine. Each animal was bled under ether anesthesia and sacrificed on days 3, 5, 7, and 21 postinoculation (p.i.). Animals were housed in biosafety level 3 animal facilities. Protocols for animal experiments were approved by the Animal Care and Use Committee of the National Institute of Infectious Diseases, Tokyo, Japan.

Serial in vivo passage of SARS-CoV in rats. The Frankfurt 1 isolate was serially passaged 10 times in 4-week-old female F344 rats. After intranasal inoculation, three rats were sacrificed on day 3 p.i. to collect bronchoalveolar wash fluids. Lungs were removed under sterile conditions, washed three times, and homogenized in 2 ml phosphate buffer containing 0.1% bovine serum albumin, 20 IU of penicillin G, 20 μl of streptomycin, and 1 μg of amphotericin B per ml. The wash fluid was then serially inoculated into F344 rats 10 times. At the 5th and 10th passage, wash fluids (F-ratV and F-ratX, respectively) were checked for virulence in rats. After 10 passages, lung homogenates were centrifuged at 2,000 rpm for 20 min, and the supernatant was used to infect Vero E6 cells. Cells were infected with 1 ml of the homogenates in 10 ml of MEM containing 2% fetal bovine serum. After 1 h of absorption, the inoculum was removed, and MEM containing 2% fetal bovine serum was added. Infected cell cultures were continuously incubated at 37°C with 5% CO_2. Cells were harvested 2 days after infection and treated once by freeze-thawing. After centrifugation at 2,000 rpm for 20 min, the supernatant was used as the virus inoculum (F-ratX-VeroE6).

Frankfurt 1, F-ratV, F-ratX, and F-ratX-VeroE6 were intranasally inoculated into 4-week-old female F344 rats. While still under ether anesthesia, the rats were bled and sacrificed by exsanguination on days 3, 5, 7, and 21 p.i., respectively. Three of the six rats were analyzed for virus replication and cytokine responses, and the other three were investigated histopathologically on each day. F-ratX-VeroE6 was similarly inoculated into adult F344 rats (7- to 8-month-old males purchased from Charles River, Inc., Japan). After intranasal inoculation with 100 μl of the virus, three adult rats were bled under ether anesthesia and killed by exsanguination on days 3, 5, and 7 p.i. to analyze virus replication and cytokine responses. Adult rats were also used for pathological examination on days 3, 5, 7, 14, and 21 p.i. Follow-up experiments were performed using 200 μl of strain F-ratX-VeroE6 using adult rats for pathological examination on days 3, 5, 7, and 14 p.i.

Virus isolation and titration. Tissue homogenates (20% [wt/vol]) from lung or maxilla including nasal cavity were prepared in MEM containing 2% fetal bovine serum, 50 IU of penicillin G, 50 μg of streptomycin, and 2.5 μg of amphotericin B per ml. Samples were clarified by centrifugation at 2,000 rpm for 20 min, and supernatants were inoculated onto VeroE6 cell cultures for virus isolation and titration.

Neutralizing antibody. Plasma samples were diluted twofold in a range from 1:10 to 1:320 with MEM containing 2% fetal bovine serum, 50 IU of penicillin G, 50 μg of streptomycin, and 2.5 μg of amphotericin B per ml. Each sample was mixed with the same volume of MEM containing SARS-CoV at an infectious dose of 100 $TCID_{50}$ per 100 μl, and the mixture was incubated for 1 h at 37°C for neutralization. After incubation, 100 μl of each sample was inoculated onto monolayers of Vero E6 cells in 96-well culture plates, which were incubated at 37°C with 5% CO_2. After 48 h, cells were examined for cytopathic effects (CPEs). The neutralizing antibody was determined as a reciprocal of the highest dilution at which a CPE was not observed.

Histopathology and immunohistochemistry. Animals were anesthetized and perfused with 10 ml of 10% phosphate-buffered formalin. Fixed tissues of lung, heart, kidney, liver, spleen, small and large intestine, brain, spinal cord, and maxilla including nasal cavity were routinely embedded in paraffin, sectioned, and stained with hematoxylin and eosin. Maxilla samples were decalcified in phosphate-buffered saline (PBS) (pH 7.4) plus 10% EDTA before embedding. Immunohistochemical detection of the SARS-CoV and ACE2 antigens was performed on paraffin-embedded sections. Rabbit antibodies against SARS-CoV and recombinant human ACE2 (R&D Systems, MN) were used as first antibodies. After deparaffining with xylene, sections were hydrated in ethanol and immersed in PBS. Antigens were retrieved by hydrolytic autoclaving for 20 min at 121°C in 10 mM/liter sodium citrate-sodium chloride buffer (pH 6.0). After cooling, sections were immersed in PBS. Endogenous peroxidase was blocked by 1% hydrogen peroxide in methanol for 30 min. After washing in PBS, the sections were treated with normal rabbit serum for 5 min and then incubated with antibodies against SARS-CoV or ACE2 overnight at 4°C. After three washes in PBS, the sections were incubated with biotin-conjugated anti-rabbit immunoglobulin G for 30 min at 37°C, followed by streptavidin-peroxidase for 30 min at room temperature. Peroxidase activity was developed in diaminobenzidine with hydrogen peroxide. Nuclei were counterstained by hematoxylin.

RNA extraction, RT-PCR, and sequencing. One hundred microliters of wash fluids and lung homogenates was treated with TRIzol (Invitrogen, Gaithersburg, MD) according to the manufacturer's instructions and then treated with DNase I (Promega, Madison, WI). RNA was dissolved in 20 μl RNase-free water. RNA extracted from the wash fluids and lung homogenates was used to generate cDNA. One microgram of eluted RNA samples was reverse transcribed using the ImProm-II reverse transcription (RT) system (Promega, Madison, WI) in a 20-μl reaction mixture containing 0.5 μg of random primers, 0.5 mM of deoxynucleoside triphosphates, 30 units of rRNasin RNase inhibitor, and 4 mM of $MgCl_2$. Mixtures were annealed at 25°C for 5 min and then incubated at 42°C for 60 min for extension, followed by heat inactivation at 70°C for 15 min. Reverse-transcribed products were stored at −20°C. A primer pair targeting the ORF7b region of SARS-CoV sequences (27415P [5′-CTCTTGCTGACAATAAAT-3′] and 27790N [5′-GAGAAGTTTCATGTTCGT-3′]) was used to detect deletion mutants. For PCR, 2.0 μl of cDNA was amplified in a 50-μl reaction mixture containing 0.2 μM each of forward and reverse primers and a high-fidelity PCR Master kit (Roche Diagnostics, Indianapolis, IN). PCR was performed as follows: (i) 4 min at 94°C and then (ii) 35 cycles, with 1 cycle consisting of 1 min at 94°C, 90 s at 55°C, and 2 min at 72°C. Products were analyzed by agarose gel electrophoresis. Water controls were included in each assay, and no false positives were observed in negative-control reactions.

In subsequent experiments, four pairs of primers targeted to spike coding region sequences (nucleotides 20751 to 26610) were used to analyze the virus genome from lung homogenates. Regions and primers were as follows: PCR15-2 (5′-AATACACCTACTTTAGCTGTACCCTACAAC-3′) and Sr10 (5′-ATCAC CGACTGTGACTTG-3′) for region 1, Seq51 (5′-TTGTCCGTGGTTGGGTT TTTGG-3′) and PCR16R (5′-GTAATAAAGAAACTGTATGGTAACTAGC AC-3′) for region 2, PCR17 (5′-CAGCTTGGCGCATATATTCTACTGGAAA C-3′) and Sr4 (5′-CCATTGAACTTCTGCGCA-3′) for region 3, and Sf7 (5′-C CTGACCCTCTAAAGCCA-3′) and PCR18R (5′-TCTGTAGACAACAGCAA GCACAAAACAAGC-3′) for region 4. For PCR, 1.0 μl of cDNA was amplified in a 50-μl reaction mixture containing 0.15 μM each of forward and reverse primers using the Expand Long PCR system (Roche Diagnostics, Indianapolis, IN). PCR was performed as follows: (i) 2 min at 94°C and (ii) 40 cycles, with 1 cycle consisting of 10 s at 94°C, 30 s at 55°C, and 8 min at 68°C. Correctly sized products were purified by using a QIAquick gel extraction kit (QIAGEN GmbH, Germany) and sequenced using a BigDye Terminator v3.1 Cycle Sequencing kit (Applied Biosystems, Foster City, CA). Sequencing products were analyzed by using an ABI PRISM 3700 DNA analyzer (Applied Biosystems, Foster City, CA). Both sense and antisense sequences of PCR products were sequenced at least once.

Cytokine multiplex analysis. Samples of sera and supernatants of 20% homogenates of lungs were analyzed for 10 cytokines (interleukin-1α [IL-1α], IL-1β, IL-2, IL-4, IL-6, IL-10, IL-12, tumor necrosis factor alpha [TNF-α], gamma interferon [IFN-γ], and granulocyte-macrophage colony-stimulating factor) with Luminex 200 (Luminex Co, Austin, TX) using a Rat Cytokine 10-plex antibody bead kit (BioSource International, Inc., Camarillo, CA) according to the manufacturer's instructions. Both samples were subjected to UV irradiation for 10 min and stored at −80°C. Homogenized lung tissue samples were diluted

1:1 in cell extraction buffer (10 mM Tris, pH 7.4, 100 mM NaCl, 1 mM EDTA, 1 mM EGTA, 1 mM NaF, 20 mM $Na_4P_2O_7$, 2 mM Na_3VO_4, 1% Triton X-100, 10% glycerol, 0.1% sodium dodecyl sulfate, and 0.5% deoxycholate; BioSource International, Inc., Camarillo, CA) for 30 min on ice with vortexing at 10-min intervals and centrifuged at 13,000 rpm for 10 min at 4°C. Supernatants were diluted 1:5 in assay diluent and assayed. Multiplex beads were vortexed and sonicated for 30 s, and 25 μl was added to each well of a 96-well filter plate and washed twice with wash buffer. Samples were diluted 1:2 with assay diluent and loaded onto a Millipore Multiscreen BV 96-well filter plate to which 50 μl of incubation buffer had been added to each well. Serial dilutions of cytokine standards were prepared in parallel and added to the plate. Samples were incubated on a plate shaker in the dark at room temperature for 2 h. The plate was applied to a Millipore Multiscreen vacuum manifold and washed twice with 200 μl wash buffer, and 100 μl of biotinylated anti-rat multicytokine detector antibody was added to each well. The plate was shaken again as described above for 1 h, applied to a Millipore Multiscreen vacuum manifold, and washed twice with 200 μl wash buffer. One hundred microliters of streptavidin R-phycoerythrin was added directly to each well, and the plate was shaken again as described above for 30 min, applied to the vacuum manifold, and washed twice. One hundred microliters of wash buffer was added to each well, and the plate was shaken for 3 min. The assay plate was analyzed using the Bio-Plex Luminex 100 XYP instrument. Cytokine concentrations were calculated using Bio-Plex Manager 3.0 software with a five-parameter curve-fitting algorithm applied for standard curve calculations.

Infection of rat ACE2-expressing CHO cells with in vivo-passaged SARS-CoV. Rat ACE2 cDNA was amplified by PCR from reverse-transcribed rat kidney RNA using primers mACE2f2 (5′-TTGCTCAGTGGATGGGATCTTGGC-3′) and ratACE2r1 (5′-GCATACAGTAAAATGACGACGAGTG-3′) and cloned into a pcDNA 3.1(+) vector (Invitrogen, Grand Island, NY). A variant rat ACE2 gene with amino acid residues 82 to 84 (NYS) altered to residues corresponding to human ACE2 (MYP) was generated as described previously by Li et al. (20) and cloned into pcDNA 3.1(+). CHO cells were transfected with plasmids encoding either form. Cells were infected with the Frankfurt 1 isolate or F-ratX-VeroE6 at a multiplicity of infection of 0.002, and culture supernatants were harvested 72 h p.i. for virus titration.

Molecular modeling of a complex of rat-passaged SARS-CoV spike protein and rat ACE2. To predict the three-dimensional (3-D) structure of the receptor binding domain of rat-passaged SARS-CoV spike protein complexed with rat ACE2, we used the crystal structure of the receptor binding domain of SARS-CoV spike protein/human ACE2 complex at a 2.9-Å resolution (Protein Data Bank accession number 2AJF) (18) as a template for homology modeling. 3-D models were constructed independently by a homology modeling technique using MOE-Align and MOE-Homology in the Molecular Operating Environment (MOE) (Chemical Computing Group Inc., Canada) as described previously (11). 3-D structures were thermodynamically optimized by energy minimization using MOE and an AMBER99 force field (29). Physically unacceptable local structures of optimized 3-D models were further refined using the Ramachandran plot program packaged in MOE.

Statistical analysis. All data were analyzed by Student's *t* test.

RESULTS

Enhanced virulence of SARS-CoV after serial in vivo passage in rats. Three days after intranasal inoculation with the Frankfurt 1 isolate of SARS-CoV, histopathological lesions in lungs of young F344 rats (4-week-old females, three rats per group) were mild, and virus antigen-positive cells were rarely seen (Fig. 1A). During 10 serial passages of the Frankfurt 1 isolate, the virus was consistently identified in the maxillar tissue, including the nasal cavity, lung tissue, and lung fluids (Fig. 1B). In nasal wash fluids, infectious virus was not detectable after the fourth passage.

It has been reported that a variant of the Frankfurt 1 isolate emerged in which 45 nucleotides (nucleotides 27670 to 27714) are deleted within ORF7b upon replication in cell culture (36). Thus, the Frankfurt 1 isolate used in the present study was a mixture of the original virus without the deletion and a variant carrying the deletion (Fig. 1C). A variant with the deletion in the ORF7b region was detected in nasal and lung washes of

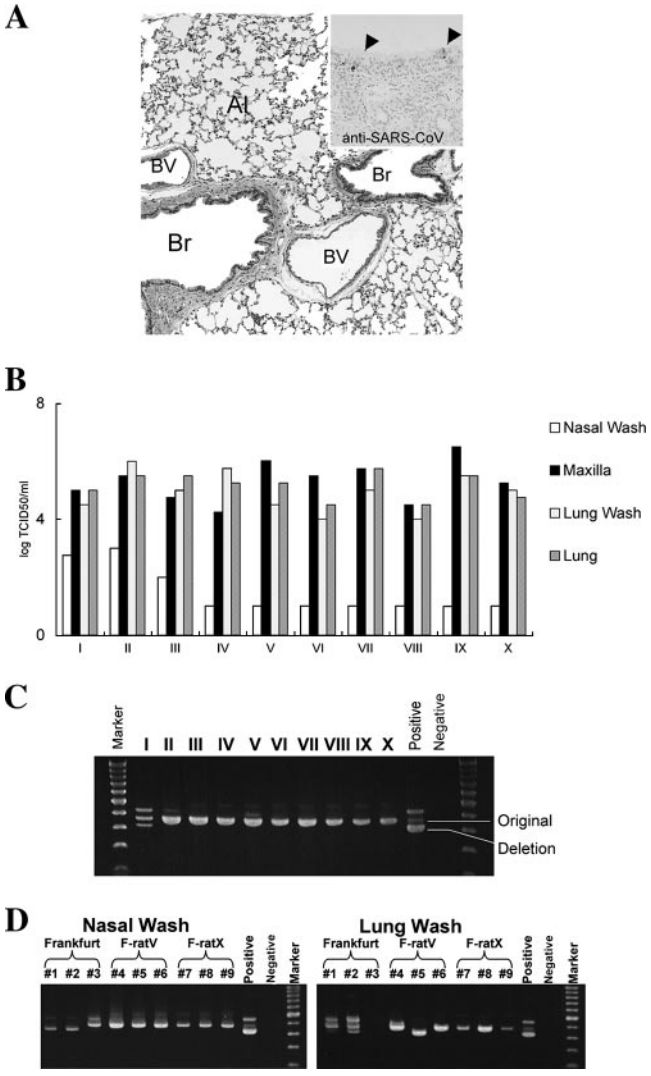

FIG. 1. Experimental infection and serial in vivo passages of SARS-CoV in young F344 rats (4-week-old females; $n = 3$). (A) Hematoxylin- and eosin-stained tissue section of lung. After intranasal inoculation with the Frankfurt 1 isolate, no inflammatory reaction in bronchi was observed. A few virus-positive cells in bronchi were seen by immunohistochemistry using SARS-CoV-specific antibody (inset, arrowheads). Br, bronchi; Al, alveoli; BV, blood vessel (magnification, ×20; inset magnification, ×40). (B) Virus titers were detected in the maxilla including nasal cavity and lung tissue homogenates and lung wash fluids following 10 serial passages. The detection limit was $10^{1.5}$ $TCID_{50}$/g of tissue. (C) DNA of serially passaged virus was amplified by RT-PCR of lung wash fluids using primers specific for ORF7b-encoding cDNA. No ORF7b deletion mutant was replicated during the serial passage. Positive indicates that the Frankfurt 1 isolate was amplified by RT-PCR; negative indicates that distilled water was used as a negative control. (D) Viral DNA was amplified by RT-PCR of nasal and lung wash fluids on day 3 p.i. using ORF7b primers. A 45-nucleotide in-frame deletion in ORF7b was detected in nasal and lung wash fluid from one animal (animal 3) and two animals (animals 1 and 2) after infection with the Frankfurt 1 isolate, respectively. F-ratV and F-ratX virus were passaged 5 and 10 times serially, respectively. The same positive and negative controls were used in C.

Frankfurt 1-infected rats; however, during serial passage in vivo, that variant was not detected (Fig. 1C and D). Replication and pathogenicity of the 5th and 10th serially passaged viruses (referred to as F-ratV and F-ratX, respectively) in the

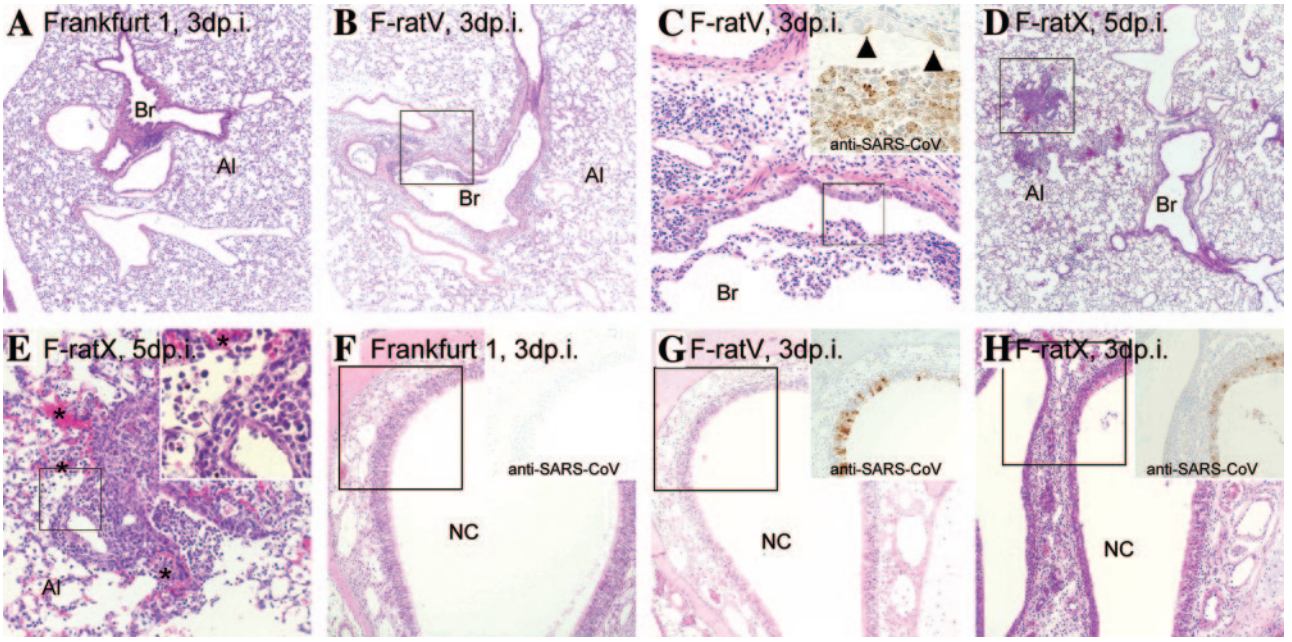

FIG. 2. Histopathologies of lung (A to E) and nasal cavity (F to H) in young F344 rats (4-week-old females; $n = 3$) after intranasal inoculation with serially passaged virus. Br, bronchi; Al, alveoli; NC, nasal cavity. (A) No inflammatory infiltrates in lung after inoculation with the Frankfurt 1 isolate were observed on day 3 p.i. (hematoxylin and eosin staining) (magnification, ×10). (B and C) Slight inflammatory reactions around bronchioles were observed in F344 rats after intranasal inoculation with five-times-serially-passaged Frankfurt 1 strain F-ratV on day 3 p.i. (C) Extensive cellular debris in bronchioles comprised of necrotic epithelia and inflammatory cells (magnification, ×50). Immunohistochemical staining using SARS-CoV-specific antibody detected virus antigen-positive cells in bronchioles and epithelial cells (C, inset) (immunohistochemistry) (magnification, ×100). (D and E) Expanded inflammatory reactions around bronchioles and the alveolar area were observed in F344 rats after inoculation with 10-times-serially-passaged Frankfurt 1 strain F-ratX on day 5 (magnifications, ×10 [D], ×50 [E], and ×100 [inset]) p.i. Small hemorrhages (*) and infiltration of lymphocytes were observed in peribronchiolar alveoli (E, inset). (F) No inflammatory reactions or virus antigen-positive cells were observed in the nasal cavity after inoculation with the Frankfurt 1 isolate on day 3 p.i. (G) Degenerated virus antigen-positive epithelial cells were observed in the nasal cavity after inoculation with F-ratV on day 3 p.i. (H) Massive inflammatory reactions and virus antigen-positive cells were observed in the nasal cavity after inoculation with F-ratX on day 3 p.i. (magnification, ×25 [F to H]).

respiratory tract of young F344 rats were higher than that seen with the original Frankfurt 1 isolate (Fig. 2 and Table 1). Young F344 rats inoculated with the original Frankfurt 1 isolate showed neither inflammatory lesions in lung nor virus antigen-positive cells in the nasal cavity on day 3 p.i. (Fig. 2A and F). After intranasal inoculation with F-ratV, virus antigens were observed immunohistochemically in the respiratory epithelia of the trachea, bronchi, and nasal cavity, which was accompanied by slight inflammatory reactions on day 3 p.i. (Fig. 2B, C, and G). More virus antigen-positive cells were seen in respiratory epithelia including the alveolar area of strain F-ratX-inoculated rats than in Frankfurt 1- or F-ratV-inoculated rats along with severe inflammatory reactions (Fig. 2D, E, and H). Inflammatory reactions, including neutrophils, macrophages, and lymphocytes, as well as microhemorrhage, were seen on day 5 p.i. (Fig. 2D and E). Thus, serial in vivo passage of virus in young rats increased SARS-CoV virulence. None of young F344 rats inoculated with the Frankfurt 1 isolate, F-ratV, or F-ratX showed any obvious clinical signs, and they survived until the observation period.

Increased pathogenicity of serially passaged SARS-CoV in adult rats. In humans, advanced age is associated with greater mortality in SARS patients. Thus, we analyzed potential differences in clinical and pathological features following infection of young (4-week-old females) and adult (7- to 8-month-old males) rats with F-ratX. Since quantities of the F-ratX

TABLE 1. Experimental infection with SARS-CoV in F344 rats

Animal age	Virus strain (100-μl inoculum)	No. of animals with inflammatory reaction/total no. of animals (no. of virus-positive animals/total no. of animals)[a]						No. of neutralization antibody-positive animals/ total no. of animals (titers of antibody to Frankfurt)
		3 days p.i.		7 day p.i.		21 days p.i.		
		Nasal cavity	Lung	Nasal cavity	Lung	Nasal cavity	Lung	
4 wk	Frankfurt	0/3 (1/3)	0/3 (0/3)	0/3 (0/3)	0/3 (0/3)	0/3 (0/3)	0/3 (0/3)	3/3 (2^6, 2^7, 2^7)
4 wk	F-ratX-VeroE6	3/3 (3/3)	3/3 (3/3)	3/3 (3/3)	3/3 (3/3)	0/5 (0/5)	4/5 (0/5)	5/5 (2^7, 2^7, 2^7, 2^8, $<2^8$)
7-8 mo	F-ratX-VeroE6	3/3 (3/3)	3/3 (3/3)	NE	3/3 (2/3)	NE	2/2 (0/2)	2/2[b] (2^7, $<2^8$)

[a] NE, not examined.
[b] Sera were collected on day 14 p.i.

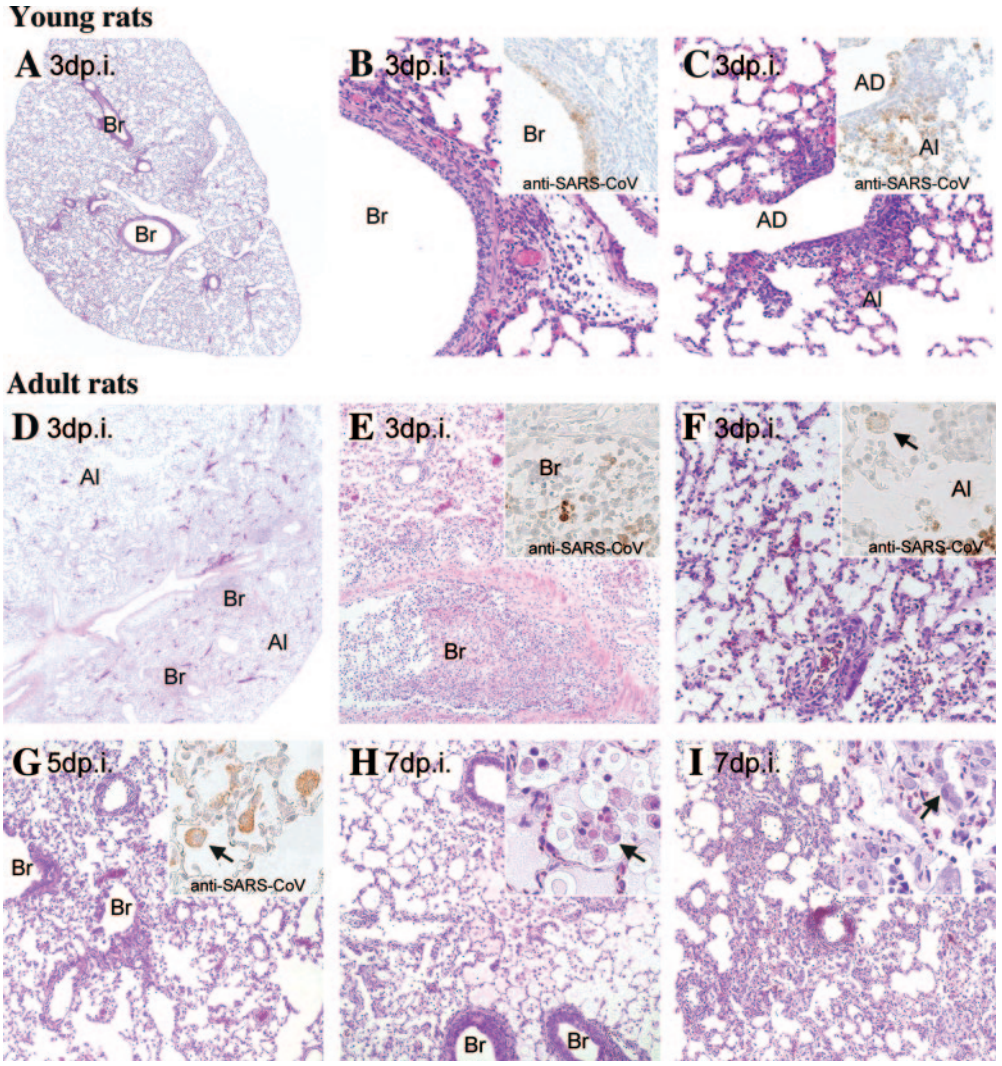

FIG. 3. Histopathological findings in lungs of young and adult F344 rats after intranasal infection with 10-times-serially-passaged SARS-CoV strain F-ratX-VeroE6 on days 3, 5, and 7 p.i. ($n = 3$). Br, bronchi; Al, alveoli; AD, alveolar duct. (A to C) Inflammatory reactions were observed around the bronchi with leukocytes and lymphocytes (B) and alveolar ducts and alveoli (C) of young F344 rats on day 3 p.i. Immunohistochemical staining with SARS-CoV-specific antibody detected virus antigen-positive cells in those epithelial cells (B and C, insets). (D to F) Massive inflammatory reactions with pulmonary edema and neutrophil and activated macrophage infiltrations were observed in lungs of adult F344 rats on day 3 p.i. Bronchi and alveoli were filled with extensive cellular debris comprised of necrotic epithelia and inflammatory cells (E and F). Immunohistochemical staining by SARS-CoV-specific antibody detected virus antigen-positive cells in necrotic cells and alveolar macrophages (arrow) (E and F, insets). (G) SARS-CoV antigen-positive cells in the alveolar macrophages of adult F344 rats on day 5 p.i. (H and I) Various stages of the inflammatory response and regeneration reaction in the alveoli of adult F344 rats on day 7 p.i. Necrotic macrophages (H, arrow) and effusion substances in alveoli (H, inset) are shown. Mononuclear cell infiltrations and regenerated type II alveolar cells (I, arrow) in alveoli (I, inset) are shown. Magnifications, ×5 (A and D), ×25 (E and G to I), ×50 (B, C, and F), and ×100 (E to I, insets).

preparation were limited, the virus was propagated once in Vero E6 cells (referred to as F-rat-X-VeroE6) before inoculation.

Histopathological features of the lung tissue 3 days after infection with the F-ratX-VeroE6 strain (100 μl of $10^{6.4}$ $TCID_{50}$) differed between young and adult rats (Fig. 3 and Table 1). In young rats without clinical symptoms, inflammatory infiltrates were seen around bronchi, bronchioles, and alveoli (Fig. 3A to C). Virus antigen-positive cells were located at epithelia of the bronchi, bronchioles, and alveoli at day 3 p.i. (Fig. 3B and C, inset). Inflammatory cells such as neutrophils, macrophages, and lymphocytes infiltrated around the affected respiratory tracts (Fig. 3B and C). Mild edema was seen around blood vessels (Fig. 3B). By contrast, after infection, adult rats became lethargic and showed ruffled fur and abdominal breathing. Grossly, a few lobes of the lungs showed congestion, edema, and consolidation at days 3 and 5 p.i. Furthermore, the inflammatory reaction, especially pulmonary edema, was more severe in adult than in young rats (Fig. 3D). Histopathological features of lung tissue on days 3 (Fig. 3E and F), 5 (Fig. 3G), and 7 (Fig. 3H and I) p.i. showed bronchiolitis obliterans organizing pneumonia and diffuse alveolar damage, which are observed in early phases of human SARS. The major inflammatory cells in alveoli were neutrophils and activated

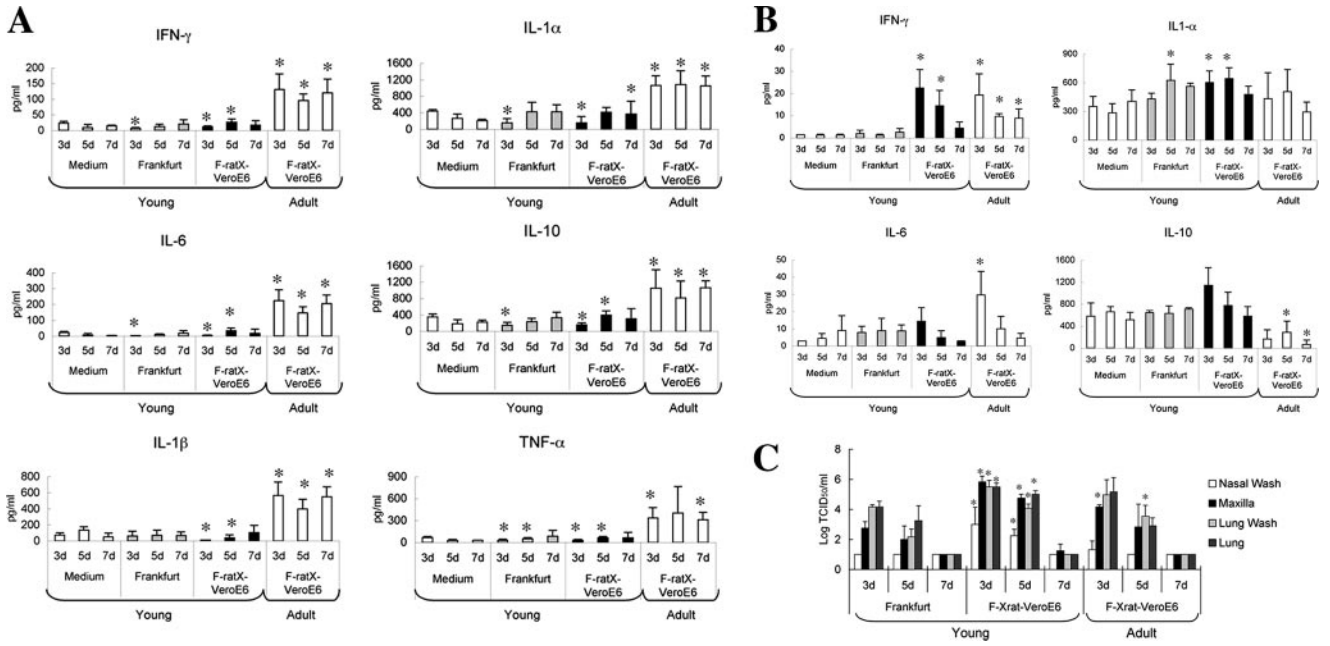

FIG. 4. Induction of inflammatory cytokines at the protein level in sera and lungs following SARS-CoV infection. (A) Cytokine levels in sera of F344 rats after infection. In F-ratX-VeroE6-inoculated adult rats ($n = 5$), serum levels of all cytokines were significantly higher than those seen in young rats ($n = 6$). Cytokine levels of adult F344 rats before infection ($n = 8$) were as follows: IFN-γ, 20.95 pg/ml; TNF-α, 183.77 pg/ml; IL-1α, 371.71 pg/ml; IL-1β, 33.64 pg/ml; IL-6, 22.54 pg/ml; IL-10, 47.07 pg/ml. (B) Cytokine levels in lung homogenates of young and adult F344 rats ($n = 3$) after infection. IFN-γ levels in F-ratX-VeroE6-inoculated young and adult rats were significantly higher than those seen in rats inoculated with the Frankfurt 1 isolate. IL-6 and IL-10 levels of F-ratX-VeroE6-inoculated adult rats were significantly higher and lower, respectively, than those seen in young rats. $*P < 0.05$ compared with medium-inoculated young F344 rats. (C) Virus titers of nasal and lung wash fluids and homogenates of maxilla including nasal cavity and lung of rats ($n = 3$) after infection. The detection limit was $10^{1.5}$ $TCID_{50}$/g of tissue.

macrophages. Fibrin deposition and hyaline membrane formation in alveolar ducts and alveoli were observed (Fig. 3F). By immunohistochemical staining, virus antigen-positive cells were alveolar macrophages and necrotic cells in the lesion (Fig. 3E to G, inset). There were no histopathological changes in the extrapulmonary tissues (brain, spinal cord, heart, liver, kidney, spleen, thymus, and gastrointestinal tract) of any of the animals examined. All the animals survived until the observation period.

Induction of cytokines in SARS-CoV-infected young and adult rats. To analyze the differences in pathogenicity seen in young and adult rats after infection with F-ratX-VeroE6, we examined cytokine levels in sera and lung homogenates (Fig. 4). Young F344 rats inoculated with medium containing 2% fetal bovine serum (100 μl) or the Frankfurt 1 isolate (100 μl of 10^7 $TCID_{50}$) served as controls. F-ratX-VeroE6 strain-infected adult rats showed significantly elevated levels of all 10 cytokines examined ($P < 0.05$) compared with mock-infected young rats (Fig. 4A). Levels of all 10 cytokines were also significantly different ($P < 0.05$) between young and adult rats infected with F-ratX-VeroE6. Adult rats showed elevated levels of IFN-γ ($P < 0.01$), IL-1α ($P = 0.01$), IL-6 ($P < 0.01$), IL-10 ($P < 0.01$), IL-12 ($P < 0.01$), granulocyte-macrophage colony-stimulating factor ($P = 0.02$), IL-4 ($P < 0.01$), and IL-1β ($P < 0.01$) after inoculation (P value between preinfected adult rats and F-ratX-VeroE6-infected adult rats on day 3 p.i.).

In lung homogenates, F-ratX-VeroE6-infected young and adult rats showed elevated levels of IFN-γ ($P = 0.012$ on day 3 and $P = 0.029$ on day 5 for young rats; $P = 0.031$ on day 3, $P < 0.01$ on day 5, and $P = 0.032$ on day 7 for adult rats) compared with mock-infected young rats (Fig. 4B). Elevated levels of IL-6 were observed early in infection in adult rats infected with F-ratX-VeroE6 compared with mock-infected rats ($P = 0.028$). Interestingly, IL-10 levels, which were significantly elevated in sera, deceased significantly in lung homogenates from adult rats infected with F-ratX-VeroE6 ($P = 0.046$ on day 5 and $P < 0.01$ on day 7 between mock-infected young rats; $P < 0.01$ on day 3, $P = 0.055$ on day 5, and $P = 0.009$ on day 7 between strain F-ratX-VeroE6-infected young rats).

Virus titers increased significantly ($P < 0.05$) in nasal and lung washes and in maxillar and lung homogenates of strain F-ratX-VeroE6-infected young rats on days 3 and 5 p.i. compared with strain Frankfurt 1-infected young rats (Fig. 4C). In contrast, in adult rats infected with the F-ratX-VeroE6 strain, virus titers increased significantly ($P < 0.05$) only in maxilla on day 3 p.i. and in lung washes on day 5 p.i. At day 7 p.i., the virus could not be isolated from the lungs of young and adult rats.

Introduction of a missense mutation within the ACE2 binding domain of the S protein of SARS-CoV during serial in vivo passage in rats. Immunohistochemical analyses revealed that ACE2 antigen-positive cells were found in respiratory epithelia of the trachea, bronchi, bronchioles, and alveolar cells of F344 rats (Fig. 5A). The ACE2 protein was most abundantly expressed on cilia of the trachea and intrapulmonary bronchus (Fig. 5A). ACE2 expression was also seen on the apical surface of bronchiolar cells and alveolar pneumocytes. During serial in vivo passage of SARS-CoV in F344 rats, virus replication sites

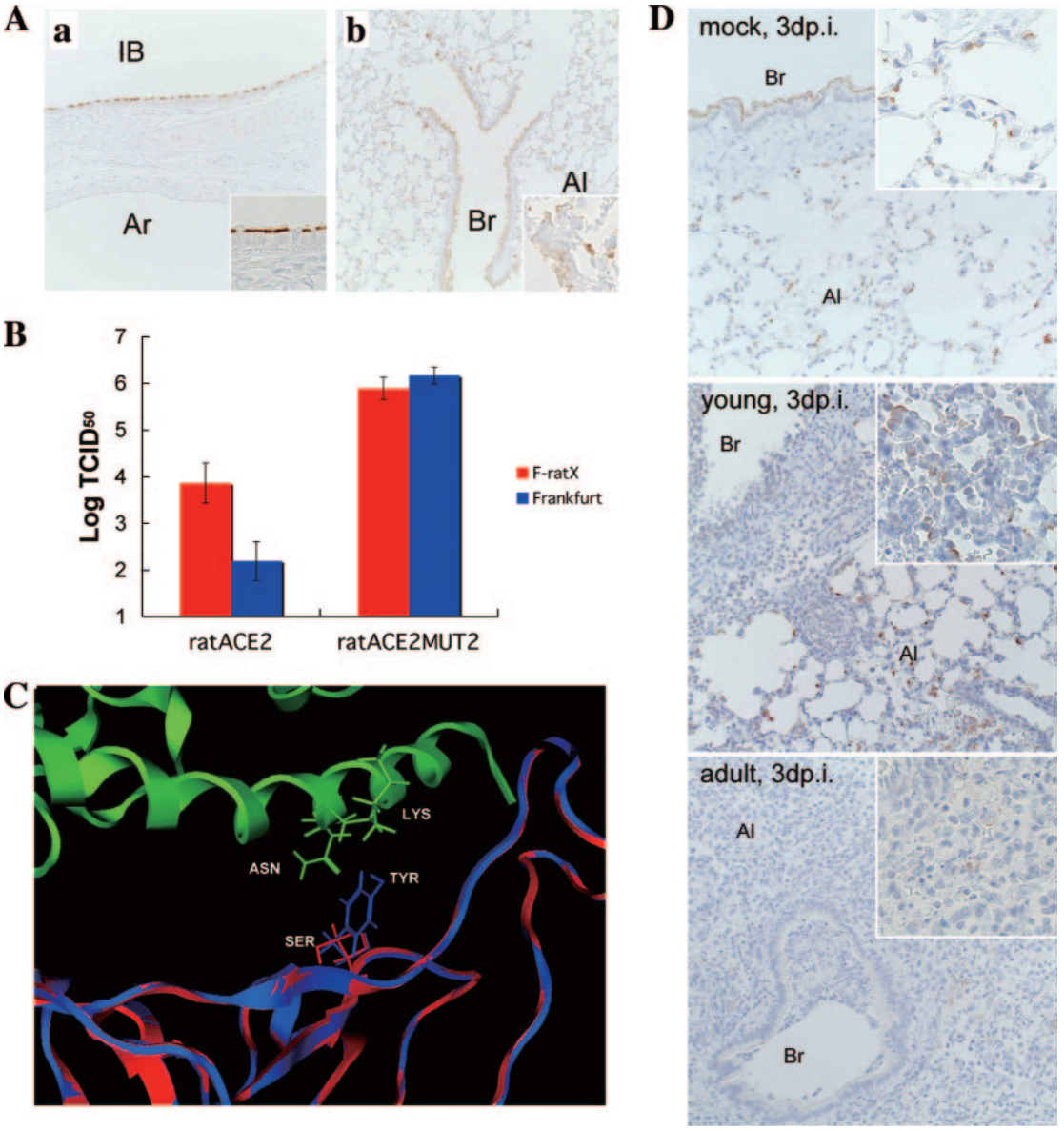

FIG. 5. Correlation of ACE2 expression and infection of serially passaged SARS-CoV in F344 rats. (A) ACE2 antigen-positive cells were detected on respiratory epithelia of the intrapulmonary bronchus (IB), bronchi (Br), and alveolar cells (Al) using immunohistochemical staining with anti-human ACE2 polyclonal antibody (magnification, ×50; inset magnification, ×100). (B) Binding of rat ACE2 to SARS-CoV in ACE2-expressing CHO cells. The F-ratX strain was detected at a higher titer than the Frankfurt 1 isolate in rat ACE2-expressing CHO cells (ratACE2) at 72 h p.i. Both Frankfurt 1 and F-ratX strains replicated in cells expressing variant forms of rat ACE2 in which residues 82 to 84 (NYS) were altered to human ACE2 (MYP) (ratACE2MUT2). The figure represents three experiments with similar results. (C) Molecular modeling of the rat-passaged SARS-CoV spike receptor binding domain complexed with rat ACE2. Green, rat ACE2; blue, Frankfurt 1 isolate; red, F-ratX strain. (D) Localization of ACE2 antigen-positive cells after infection with SARS-CoV on day 3 p.i. by staining with anti-human ACE2 polyclonal antibody. Br, bronchi; Al, alveoli. ACE2 antigen localized to alveolar cells and bronchial epithelial cells in lung of adult rats after mock infection (top, adult F344 rat after intranasal inoculation with MEM). ACE2 antigen-positive cells disappeared in affected bronchi of both young and adult rats (middle, young rat; bottom, adult F344 rat [both after intranasal inoculation with F-ratX-VeroE6]). High expression of ACE2 was found in the apical side of regenerated type II alveolar cells in lesion areas of young rats. Reduced ACE2 expression was observed in inflammatory areas of adult rats (magnification, ×50; inset magnification, ×100).

in lung extended from the bronchus to the alveolar area where ACE2-positive cells were located (Fig. 2 and 5A). ACE2 expression appeared to correlate with the extent and location of virus antigen-positive cells. To examine whether infection by rat-passaged virus is efficiently mediated by rat ACE2, F-ratX and the Frankfurt 1 isolate were inoculated onto rat ACE2-expressing CHO cells. F-ratX replicated more efficiently in these cells than the Frankfurt 1 isolate, while both viruses replicated at the same level in CHO cells expressing an ACE2 variant in which amino acid residues 82 to 84 (NYS) were replaced by the corresponding MYP motif seen in human ACE2 (Fig. 5B). Sequence analysis of the F-ratX strain re-

vealed an A-to-C point mutation at nucleotide 1325 in the region encoding the ACE2 binding site of S1. This mutation resulted in a Y-to-S amino acid change at position 442 in the S protein. The 3-D structure of a complex of the receptor binding domain of the S protein and rat ACE2 predicts that the binding interface might be altered by such a mutation (Fig. 5C). ACE2 expression was examined by immunohistochemistry in young or adult rats after infection with F-ratX-VeroE6 (Fig. 5D). ACE2 antigen-positive cells disappeared in the affected bronchi of both young and adult rats. In young rats, however, ACE2 expression was seen in regenerated type II alveolar cells. By contrast, ACE2 antigen-positive cells were rarely observed in lung lesion areas of adult rats. Thus, ACE2 expression is highly downregulated in the F-ratX-VeroE6-infected adult rats.

DISCUSSION

Our goal was to understand the pathogenesis of SARS-CoV and develop an animal model of SARS. We demonstrated that serial in vivo passage of a human isolate of SARS-CoV, Frankfurt 1, in young F344 rats resulted in the increased virulence of SARS-CoV. The increased infectivity of SARS-CoV after serial passage in F344 rats was correlated with a single amino acid change in the receptor binding domain of the S1 protein, which mediates efficient SARS-CoV binding to ACE2 receptor-expressed rat cells based on both in vitro and structural studies. Adult F344 rats showed severe pathological changes compared with young F344 rats, and those changes were similar to features of human pathology recognized in the SARS epidemic of 2003 to 2004. Here, we demonstrate that both virus and host factors are crucial for the pathogenesis of SARS in vivo.

It has been reported that a virus variant in which 45 nucleotides (nucleotides 27670 to 27714) are deleted within ORF7b emerged upon replication of the Frankfurt 1 isolate in cell culture (37). Thus, for this study, we used a mixture of the original virus and the variant carrying the deletion. The observation that a variant with the deletion was detected in Frankfurt 1-infected rat specimens but was not detected following serial in vivo passaging suggests that the ORF7b may function in viral replication in vivo.

In addition, a Y-to-S amino acid change at residue 442 of the ACE2 binding domain of the S protein occurred during serial passage of the virus in F344 rats. As we have not yet completely sequenced all of the virus genome, it is still possible that another change enhanced virus replication in the rat. However, Li et al. previously demonstrated that residues 479N and 487T within the S-protein receptor binding domain are critical for efficient interaction with human ACE2 and that these residues might be introduced into the virus by mutations during the adaptation of palm civet SARS-CoV, which has 479K and 487S, to humans (20). It seems likely that the Y-to-S mutation at S-protein residue 442 is critical for efficient infection with rat ACE2, since F-ratX replicated more efficiently than the Frankfurt 1 isolate in rat ACE2-expressing CHO cells. Moreover, the 3-D structural prediction of a complex of the S-protein receptor binding domain and rat ACE2 suggests that the binding interface is altered by the Y-to-S mutation. Increased interactions may also be responsible for efficient replication of the virus in rat, since during serial in vivo passage of the virus, replication sites in the lung extended from the bronchus, where ACE2 is most abundantly expressed, to the alveolar area, where it is expressed at a much lower level. Thus, the Y-to-S mutation at residue 442 may partly mediate the increased virulence seen in rats.

Based on immunohistochemical analysis of ACE2 expression in the lung of F344 rats, the ACE2 protein is most abundantly expressed on the cilia of trachea and intrapulmonary bronchi. ACE2 expression appears to correlate with the extent of virus replication sites. Upon infection with F-ratX-VeroE6, ACE2 antigen-positive cells disappeared in the affected bronchi of both young and adult rats. However, ACE2 was expressed in regenerated type II alveolar cells of young rats, but that expression was significantly reduced in adult rats. The downregulation of ACE2 expression by SARS-CoV infection and the presence of the SARS-CoV spike protein in vivo and in vitro have been previously reported (13). Since ACE2 negatively regulates the rennin-angiotensin system by inactivating angiotensin II, which is generated from angiotensin I by ACE, downregulation of ACE2 expression likely blocks the renninangiotensin pathway, which has a crucial role in severe acute lung injury (8, 13). Thus, the downregulation of ACE2 in the lungs of adult rats likely contributes to severe lung injury.

In F-ratX-VeroE6-infected young rats, more virus antigen-positive cells were found in the respiratory epithelia, including the alveolar area, with severe inflammatory reactions; however, rats did not show clinical symptoms of illness. On the other hand, adult rats showed clinical illness and severe pathological changes following F-ratX-VeroE6 infection. Such changes paralleled features seen in human pathologies following the SARS epidemic of the winter of 2003 to 2004 and strongly indicate that host as well as viral factors function in the pathogenesis of SARS in rats. Epidemiological studies of the SARS outbreak of 2003 to 2004 showed that advanced age was a risk factor for an adverse outcome from SARS (1, 3, 16, 27, 38). Roberts et al. previously demonstrated the efficiency of SARS-CoV replication in aged BALB/c mice (33). Our study of animals supports the observation that advanced age is a risk factor for the development of SARS.

Histopathological analysis of adult male F344 rats after F-ratX-VeroE6 infection showed severe inflammatory reactions, especially pulmonary edema. Furthermore, morphologically activated macrophages were observed in alveoli on days 3, 5, and 7 p.i. In contrast, after intranasal inoculation of young rats with F-ratX-VeroE6, inflammatory cell infiltrates consisted of leukocytes and lymphocytes on day 3 p.i. Acute lung injury caused by SARS-CoV is likely a complex pathophysiological process involving inflammatory cytokines released from activated macrophages in alveoli, leading to immune systems dysregulation (25). Our results suggest that the overinduction of inflammatory cytokines in sera and lung homogenates underlies the development of severe inflammation in adult rats. In lung homogenates in particular, IL-6 levels were increased significantly in adult rats after intranasal inoculation with F-ratX-VeroE6 on day 3 p.i.; however, IL-10 levels decreased significantly in adult rats on days 5 and 7 p.i. IL-6, an inflammatory cytokine, is produced by leukocytes, monocytes, endothelial cells, fibroblasts, and alveolar epithelial cells. Serum cytokine levels in SARS patients, particularly IL-6, are signif-

icantly elevated (40). In vitro studies suggest that SARS-CoV replication induces high levels of IL-6 compared with other respiratory viruses (26). Our findings indicate that IL-6 may be produced by predominantly infiltrated leukocytes and macrophages in injured lungs and leads to enhanced inflammatory reactions. By contrast, IL-10, an immunosuppressive cytokine of macrophages, Th2 lymphocytes, and B cells, inhibits TNF-α production and neutrophil activation in lipopolysaccharide-induced acute lung injury and leads to decreases in lung tissue injury (9). Therefore, decreased IL-10 levels in the lung may be responsible for the loss of protective mechanisms, enabling the inflammatory response to continue. It was reported that IL-10 levels increase in the convalescent phase in SARS patients (25). It is currently unclear why elevated cytokine levels are observed in adult rats following F-ratX-VeroE6 infection, since virus replication rates are decreased compared to those for infected young rats. However, our in vivo study suggests that excess cytokine activation may play a key role in the clinical and pathological features of SARS.

In conclusion, we developed an animal model of SARS after SARS-CoV was passaged 10 times in F344 rats and then propagated in Vero E6 cells (F-ratX-VeroE6). This study suggests that both virus and host factors underlie the pathogenesis of SARS. Such an in vivo comparative study of immune responses of young and adult rats using the adapted virus could be useful in further understanding the pathogenesis of SARS, and this model described here should be useful to evaluate vaccine candidates and antiviral agents against SARS-CoV infection.

ACKNOWLEDGMENTS

We thank J. Ziebuhr, Institute of Virology and Immunology, University of Würzburg, Würzburg, Germany, for kindly supplying the Frankfurt 1 isolate. We also thank M. Fujino, I. Hatano, and M. Kataoka, Department of Pathology, National Institute of Infectious Diseases, for technical assistance.

This work was partly supported by a Grant-in Aid for Research on Emerging and Re-Emerging Infectious Diseases from the Ministry of Health, Labor, and Welfare, Japan, and a Grant-in-Aid for Scientific Research from the Ministry of Education, Culture, Sports, Science, and Technology, Japan.

REFERENCES

1. **Booth, C. M., L. M. Matukas, G. A. Tomlinson, A. R. Rachlis, D. B. Rose, H. A. Dwosh, S. L. Walmsley, T. Mazzulli, M. Avendano, P. Derkach, I. E. Ephtimios, I. Kitai, B. D. Mederski, S. B. Shadowitz, W. L. Gold, L. A. Hawryluck, E. Rea, J. S. Chenkin, D. W. Cescon, S. M. Poutanen, and A. S. Detsky.** 2003. Clinical features and short-term outcomes of 144 patients with SARS in the greater Toronto area. JAMA **289:**2801–2809.
2. **Bukreyev, A., E. W. Lamirande, U. J. Buchholz, L. N. Vogel, W. R. Elkins, M. St. Claire, B. R. Murphy, K. Subbarao, and P. L. Collins.** 2004. Mucosal immunisation of African green monkeys (Cercopithecus aethiops) with an attenuated parainfluenza virus expressing the SARS coronavirus spike protein for the prevention of SARS. Lancet **363:**2122–2127.
3. **Donnelly, C. A., A. C. Ghani, G. M. Leung, A. J. Hedley, C. Fraser, S. Riley, L. J. Abu-Raddad, L. M. Ho, T. Q. Thach, P. Chau, K. P. Chan, T. H. Lam, L. Y. Tse, T. Tsang, S. H. Liu, J. H. Kong, E. M. Lau, N. M. Ferguson, and R. M. Anderson.** 2003. Epidemiological determinants of spread of causal agent of severe acute respiratory syndrome in Hong Kong. Lancet **361:**1761–1766.
4. **Drosten, C., S. Günther, W. Preiser, S. van der Werf, H. R. Brodt, S. Becker, H. Rabenau, M. Panning, L. Kolesnikova, R. A. M. Fouchier, A. Berger, A. M. Burguière, J. Cinatl, M. Eickmann, N. Escriou, K. Grywna, S. Kramme, J. C. Mariuguerra, S. Müller, V. Rickerts, M. Stürmer, S. Vieth, H. D. Klenk, A. D. M. E. Osterhaus, H. Schmitz, and H. W. Doerr.** 2003. Identification of a novel coronavirus in patients with severe acute respiratory syndrome. N. Engl. J. Med. **348:**1967–1976.
5. **Fouchier, R. A. M., T. Kuiken, M. Schutten, G. van Amerongen, G. J. J. van Doornum, B. G. van den Hoogen, M. Peiris, W. Lim, K. Stöhr, and A. D. M. E. Osterhaus.** 2003. Koch's postulates fulfilled for SARS virus. Nature **423:**240.
6. **Gao, W., A. Tamin, A. Soloff, L. D'Aiuto, E. Nwanegbo, P. D. Robbins, W. J. Bellini, S. Barratt-Boyes, and A. Gambotto.** 2003. Effects of a SARS-associated coronavirus vaccine in monkeys. Lancet **362:**1895–1896.
7. **Greenough, T. C., A. Carville, J. Coderre, M. Somasundaran, J. L. Sullivan, K. Luzuriaga, and K. Mansfield.** 2005. Pneumonitis and multi-organ system disease in common marmosets (Callithrix jacchus) infected with the severe acute respiratory syndrome-associated coronavirus. Am. J. Pathol. **167:**455–463.
8. **Imai, Y., K. Kuba, S. Rao, Y. Huan, F. Guo, B. Guan, P. Yang, R. Sarao, T. Wada, H. Leong-Poi, M. A. Crackower, A. Fukamizu, C. C. Hui, L. Hein, S. Uhlig, A. S. Slutsky, C. Jiang, and J. M. Penninger.** 2005. Angiotensin-converting enzyme 2 protects from severe acute lung failure. Nature **436:**112–116.
9. **Inoue, G.** 2000. Effect of interleukin-10 (IL-10) on experimental LPS-induced acute lung injury. J. Infect. Chemother. **6:**51–60.
10. **Jia, H. P., D. C. Look, L. Shi, M. Hickey, L. Pewe, J. Netland, M. Farzan, C. Wohlford-Lenane, S. Perlman, and P. B. McCray, Jr.** 2005. ACE2 receptor expression and severe acute respiratory syndrome coronavirus infection depend on differentiation of human airway epithelia. J. Virol. **79:**14614–14621.
11. **Kinomoto, M., M. Yokoyama, H. Sato, A. Kojima, T. Kurata, K. Ikuta, T. Sata, and K. Tokunaga.** 2005. Amino acid 36 in the human immunodeficiency virus type 1 gp41 ectodomain controls fusogenic activity: implications for the molecular mechanism of virus escape from a fusion inhibitor. J. Virol. **79:**5996–6004.
12. **Ksiazek, T. G., D. Erdman, C. S. Goldsmith, S. R. Zaki, T. Peret, S. Emery, S. Tong, C. Urbani, J. A. Comer, W. Lim, P. E. Rollin, S. F. Dowell, A.-E. Ling, C. D. Humphrey, W.-J. Shieh, J. Guarner, C. D. Paddock, P. Rota, B. Fields, J. DeRisi, J. Y. Yang, N. Cox, J. M. Hughes, J. W. LeDuc, W. J. Bellini, L. J. Anderson, and the SARS Working Group.** 2003. A novel coronavirus associated with severe acute respiratory syndrome. N. Engl. J. Med. **348:**1953–1966.
13. **Kuba, K., Y. Imai, S. Rao, H. Gao, F. Guo, B. Guan, Y. Huan, P. Yang, Y. Zhang, W. Deng, L. Bao, B. Zhang, G. Liu, Z. Wang, M. Chappell, Y. Liu, D. Zheng, A. Leibbrandt, T. Wada, A. S. Slutsky, D. Liu, C. Qin, C. Jiang, and J. M. Penninger.** 2005. A crucial role of angiotensin converting enzyme 2 (ACE2) in SARS coronavirus-induced lung injury. Nat. Med. **11:**875–879.
14. **Kuiken, T., R. A. M. Fouchier, M. Schutten, G. F. Rimmelzwaan, G. van Amerongen, D. van Riel, J. D. Laman, T. de Jong, G. van Doornum, W. Lim, A. E. Ling, P. K. S. Chan, J. S. Tam, M. C. Zambon, R. Gopal, C. Drosten, S. van der Werf, N. Escriou, J. C. Manuguerra, K. Stöhr, J. S. M. Peiris, and A. D. M. E. Osterhaus.** 2003. Newly discovered coronavirus as the primary cause of sever acute respiratory syndrome. Lancet **362:**263–270.
15. **Lai, M. M. C., and K. V. Holmes.** 2001. Coronaviridae: the viruses and their replication, p. 1163–1185. *In* D. M. Knipe and P. M. Howley (ed.), Fields virology, 4th ed. Lippincott Williams & Wilkins, Philadelphia, PA.
16. **Lee, N., D. Hui, A. Wu, P. Chan, P. Cameron, G. M. Joynt, A. Ahuja, M. Y. Yung, B. Sc, C. B. Leung, K. F. To, S. F. Lui, C. C. Szeto, S. Chung, and J. J. Y. Sung.** 2003. A major outbreak of severe acute respiratory syndrome in Hong Kong. N. Engl. J. Med. **348:**1986–1994.
17. **Li, B. J., Q. Tang, D. Cheng, C. Qin, F. Y. Xie, Q. Wei, J. Xu, Y. Liu, B. J. Zheng, M. C. Woodle, N. Zhong, and P. Y. Lu.** 2005. Using siRNA in prophylactic and therapeutic regimens against SARS coronavirus in Rhesus macaque. Nat. Med. **9:**944–951.
18. **Li, F., W. Li, M. Farzan, and S. C. Harrison.** 2005. Structure of SARS coronavirus spike receptor-binding domain complexed with receptor. Science **309:**1864–1868.
19. **Li, W., M. J. Moore, N. Vasilieva, J. Sui, S. K. Wong, M. A. Berne, M. Somasundaran, J. L. Sullivan, K. Luzuriaga, T. C. Greenough, H. Choe, and M. Farzan.** 2003. Angiotensin-converting enzyme 2 is a functional receptor for the SARS coronavirus. Nature **426:**450–454.
20. **Li, W., C. Zhang, J. Sui, J. H. Kuhn, M. J. Moore, S. Luo, S. K. Wong, I. C. Huang, K. Xu, N. Vasilieva, A. Murakami, Y. He, W. A. Marasco, Y. Guan, H. Choe, and M. Farzan.** 2005. Receptor and viral determinants of SARS-coronavirus adaptation to human ACE2. EMBO J. **24:**1634–1643.
21. **Li, W., T. C. Greenough, M. J. Moore, N. Vasilieva, M. Somasundaran, J. L. Sullivan, M. Farzan, and H. Choe.** 2004. Efficient replication of severe acute respiratory syndrome coronavirus in mouse cells is limited by murine angiotensin-converting enzyme 2. J. Virol. **78:**11429–11433.
22. **Liang, L., C. He, M. Lei, S. Li, Y. Hao, H. Zhu, and Q. Duan.** 2005. Pathology of guinea pigs experimentally infected with a novel reovirus and coronavirus isolated from SARS patients. DNA Cell Biol. **24:**485–490.
23. **Martina, B. E., B. L. Haagmans, T. Kuiken, R. A. Fouchier, G. F. Rimmelzwaan, G. Van Amerongen, J. S. Peiris, W. Lim, and A. D. Osterhaus.** 2003. SARS virus infection of cats and ferrets. Nature **425:**915.
24. **McAuliffe, J., L. Vogel, A. Roberts, G. Fahle, S. Fischer, W. Shieh, E. Butler, S. Zaki, M. S. Claire, B. Murphy, and K. Subbarao.** 2004. Replication of SARS coronavirus administered into the respiratory tract of African green, rhesus and cynomolgus monkeys. Virology **330:**8–15.
25. **Nicholls, J. M., L. L. Poon, K. C. Lee, W. F. Ng, S. T. Lai, C. Y. Leung, C. M. Chu, P. K. Hui, K. L. Mak, W. Lim, K. W. Yan, K. H. Chan, N. C. Tsang, Y.**

Guan, K. Y. Yuen, and J. S. Peiris. 2003. Lung pathology of fatal severe acute respiratory syndrome. Lancet **361:**1773–1778.
26. **Okabayashi, T., H. Kariwa, S. Yokota, S. Iki, T. Indoh, N. Yokosawa, I. Takashima, H. Tsutsumi, and N. Fujii.** 2006. Cytokine regulation in SARS coronavirus infection compared to other respiratory virus infections. J. Med. Virol. **78:**417–424.
27. **Peiris, J. S., C. M. Chu, V. C. Cheng, K. S. Chan, I. F. Hung, L. L. Poon, K. I. Law, B. S. Tang, T. Y. Hon, C. S. Chan, K. H. Chan, J. S. Ng, B. J. Zheng, W. L. Ng, R. W. Lai, Y. Guan, K. Y. Yuen, and the HKU/UCH SARS Study Group.** 2003. Clinical progression and viral load in a community outbreak of coronavirus-associated SARS pneumonia: a prospective study. Lancet **361:** 1767–1772.
28. **Peiris, J. S. M., S. T. Lai, L. L. M. Poon, Y. Guan, L. Y. C. Yam, W. Lim, J. Nicholls, W. K. S. Yee, W. W. Yan, M. T. Cheung, V. C. C. Cheng, K. H. Chan, D. N. C. Tsang, R. W. H. Yung, T. K. Ng, K. Y. Yuen, and Members of the SARS Study Group.** 2003. Coronavirus as a possible cause of severe acute respiratory syndrome. Lancet **361:**1319–1325.
29. **Ponder, J. W., and D. A. Case.** 2003. Force fields for protein simulations. Adv. Protein Chem. **66:**27–85.
30. **Qin, C., J. Wang, Q. Wei, M. She, W. A. Marasco, H. Jiang, X. Tu, H. Zhu, L. Ren, H. Gao, L. Guo, L. Huang, R. Yang, Z. Cong, L. Guo, Y. Wang, Y. Liu, Y. Sun, S. Duan, J. Qu, L. Chen, W. Tong, L. Ruan, P. Liu, H. Zhang, J. Zhang, H. Zhang, D. Liu, Q. Liu, T. Hong, and W. He.** 2005. An animal model of SARS produced by infection of Macaca mulatta with SARS coronavirus. J. Pathol. **206:**251–259.
31. **Qin, E., H. Shi, L. Tang, C. Wang, G. Chang, Z. Ding, K. Zhao, J. Wang, Z. Chen, M. Yu, B. Si, J. Liu, D. Wu, X. Cheng, B. Yang, W. Peng, Q. Meng, B. Liu, W. Han, X. Yin, H. Duan, D. Zhan, L. Tian, S. Li, J. Wu, G. Tan, Y. Li, Y. Li, Y. Liu, H. Liu, F. Lv, Y. Zhang, X. Kong, B. Fan, T. Jiang, S. Xu, X. Wang, C. Li, X. Wu, Y. Deng, M. Zhao, and Q. Zhu.** 2005. Immunogenicity and protective efficacy in monkeys of purified inactivated Vero-cell SARS vaccine. Vaccine **24:**1028–1034.
32. **Roberts, A., L. Vogel, J. Guarner, N. Hayes, B. Murphy, S. Zaki, and K. Subbarao.** 2005. Severe acute respiratory syndrome coronavirus infection of golden Syrian hamsters. J. Virol. **79:**503–511.
33. **Roberts, A., C. Paddock, L. Vogel, E. Butler, S. Zaki, and K. Subbarao.** 2005. Aged BALB/c mice as a model for increased severity of severe acute respiratory syndrome in elderly humans. J. Virol. **79:**5833–5838.
34. **Rowe, T., G. Gao, R. J. Hogan, R. G. Crystal, T. G. Voss, R. L. Grant, P. Bell, G. P. Kobinger, N. A. Wivel, and J. M. Wilson.** 2004. Macaque model for severe acute respiratory syndrome. J. Virol. **78:**11401–11404.
35. **Sims, A. C., R. S. Baric, B. Yount, S. E. Burkett, P. L. Collins, and R. J. Pickles.** 2005. Severe acute respiratory syndrome coronavirus infection of human ciliated airway epithelia: role of ciliated cells in viral spread in the conducting airways of the lungs. J. Virol. **79:**15511–15524.
36. **Snijder, E. J., P. J. Bredenbeek, J. C. Dobbe, V. Thiel, J. Ziebuhr, L. L. Poon, Y. Guan, M. Rozanov, W. J. Spaan, and A. E. Gorbalenya.** 2003. Unique and conserved features of genome and proteome of SARS-coronavirus, an early split-off from the coronavirus group 2 lineage. J. Mol. Biol. **331:**991–1004.
37. **Thiel, V., K. A. Ivanov, A. Putics, T. Hertzig, B. Schelle, S. Bayer, B. Weissbrich, E. J. Snijder, H. Rabenau, H. W. Doerr, A. E. Gorbalenya, and J. Ziebuhr.** 2003. Mechanisms and enzymes involved in SARS coronavirus genome expression. J. Gen. Virol. **84:**2305–2315.
38. **Tsui, P. T., M. L. Kwok, H. Yuen, and S. T. Lai.** 2003. Severe acute respiratory syndrome: clinical outcome and prognostic correlates. Emerg. Infect. Dis. **9:**1064–1069.
39. **Weingartl, H. M., J. Copps, M. A. Drebot, P. Marszal, G. Smith, J. Gren, M. Andova, J. Pasick, P. Kitching, and M. Czub.** 2004. Susceptibility of pigs and chickens to SARS coronavirus. Emerg. Infect. Dis. **10:**179–184.
40. **Zhang, Y., J. Li, Y. Zhan, L. Wu, X. Yu, W. Zhang, L. Ye, S. Xu, R. Sun, Y. Wang, and J. Lou.** 2004. Analysis of serum cytokines in patients with severe acute respiratory syndrome. Infect. Immun. **72:**4410–4415.